Materials Letters 237 (2019) 216–219

Contents lists available at ScienceDirect

Materials Letters

journal homepage: www.elsevier.com/locate/mlblue

# Surface nanocrystallization of Cu-Cr alloy by a high power density continuous laser beam

Litian Zhang [a,b], Gang Yu [a,c,*], Xiuli He [a,b], Shaoxia Li [a], Chongxin Tian [a,b]

[a] Institute of Mechanics, Chinese Academy of Sciences, Beijing 100190, China
[b] School of Engineering Science, University of Chinese Academy of Sciences, Beijing 100049, China
[c] Center of Materials Science and Optoelectronics Engineering, University of Chinese Academy of Sciences, Beijing 100049, China

ARTICLE INFO

*Article history:*
Received 2 November 2018
Received in revised form 16 November 2018
Accepted 18 November 2018
Available online 19 November 2018

*Keywords:*
Laser surface melting
Cu-Cr alloy
Solidification
Microstructure
Surface nanocrystallization

ABSTRACT

A nanostructured surface layer of ~300 μm thickness was fabricated on Cu-30Cr (wt%) hypereutectic alloy by a continuous laser beam with high power density ($1.08 \times 10^7$ W/cm$^2$). The average grain size of Cr-rich particles was refined to ~40 nm, and the solid solubility limit of Cr in Cu was extended to 1.96 at. %. Experimental results show that the dispersion of nano-sized Cr-rich spheroids in Cu-rich matrix was attributed to the Brownian motion of Cr-rich spheroids, and the high cooling rate ($5.75 \times 10^6$ K/s) during liquid phase separation which inhibits the collisions between Cr-rich spheroids.


## 1. Introduction

Surfaces of engineering materials or components are the sites where failures frequently originate. In the past decades, surface nanocrystallization has been adopted to improve the overall mechanical properties and service behaviors. Severe plastic deformation [1,2], electron beam [3] or laser beam [4,5] were applied to transfer surface layer of metallic materials into nanostructured state. Among them, with the merits of strong metallurgical bonding, fast processing speed and high controllability, laser surface melting (LSM) technique has been widely employed to surface nanocrystallization of low carbon steel [6,7], Al alloys [8] while keeping the composition unchanged. However, LSM of Cu-Cr alloys was extremely challenging due to high reflectivity to infrared wavelength laser, high thermal conductivity and low wettability, reports of surface nanocrystallization of Cu-Cr by LSM were rare.

In this study, surface nanocrystallization of Cu-Cr alloy was achieved by a continuous laser beam with high power density ($Q = 1.08 \times 10^7$ W/cm$^2$). Thermally induced surface nanocrystallization via liquid phase separation (LPS) during fast heating and rapid solidification in LSM was investigated, and grain refinement mechanism of LSM treated Cu-Cr alloy was explored.

## 2. Experimental

Cu-30Cr (wt%) alloy prepared by powder metallurgy method was used as experimental material, and the average surface roughness was 1.6 ± 0.4 μm. A continuous Nd:YAG laser with a wavelength of 1.064 μm was selected in this study. The laser power density was $1.08 \times 10^7$ W/cm$^2$, which was much higher than the conventionally recognized power density for LSM ($10^5$ W/cm$^2$) [9]. Other parameters were as follows:scanning speed 8 m/min, beam diameter 100 μm, track distance 70 μm. A circulating water cooling system was assembled at the bottom of the sample to keep the bottom temperature at 288 K. The whole process was conducted in a high purity argon atmosphere box (content: $O_2$ < 10 ppm, $H_2O$ < 10 ppm) to avoid oxidation.

After LSM, the sample was cut perpendicular to the scanning direction. The microstructure was observed by ZEISS EVO-18 scanning electron microscopy (SEM) equipped with a backscattered electron detector (BSE), and JEM-2100F transmission electron microscopy (TEM). The phase constituents were analyzed by X-ray diffractometer (XRD, with Cu Kα radiation).

## 3. Results and discussion

Fig. 1a presents the XRD patterns of Cu-Cr alloy before and after LSM. No changes in crystallographic orientations of Cu and Cr were detected, and no intermetallic phase was formed. The phase

* Corresponding author.
*E-mail address:* gyu@imech.ac.cn (G. Yu).

https://doi.org/10.1016/j.matlet.2018.11.108
0167-577X/

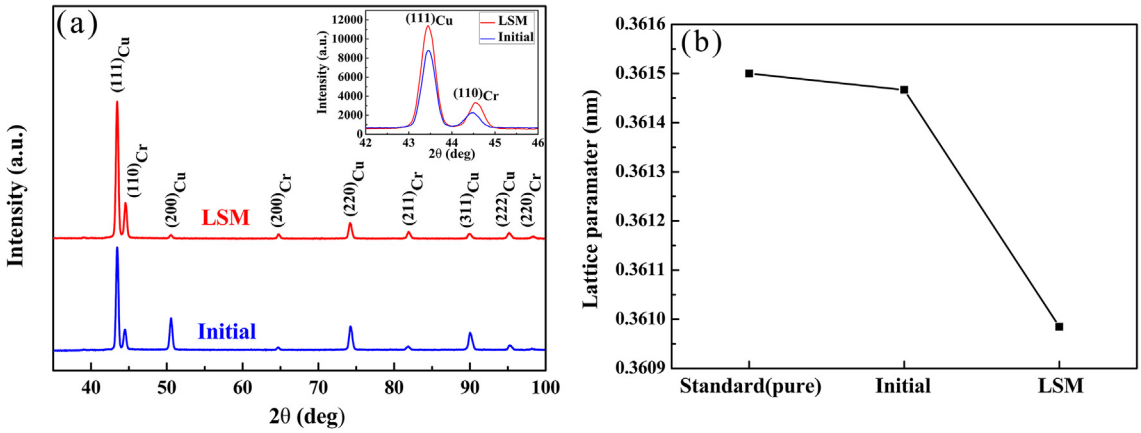


**Fig. 1.** (a) XRD measurements on the raw-material and after LSM (b) Cu lattice parameter.

constituents indicated as a body centered cubic (BCC) α-Cr and a face centered cubic (FCC) ε-Cu. The crystallite size D was determined by Scherrer formula [10]:

$$D = \frac{0.9\lambda}{B \cdot \cos\theta} \quad (1)$$

where λ = 0.15405 nm is the wavelength of the X-ray, B is the peak width at half the maximum intensity and θ is the Bragg diffraction angle. Thus, the crystallite size of α-Cr was ~36.7 nm. As indicated from the enlarged image of Cu (1 1 1) and Cr (1 1 0) peaks in Fig. 1a, the peaks of LSM treated sample become broadening and the relative intensity ratios reduced, revealing that the Cr atoms were dissolved in Cu. Lattice parameter of Cu was shown in Fig. 1b, the value decreased after LSM treatment. Lattice parameter variation (Δa) due to non-equilibrium solidification was defined by:

$$\Delta a = a_{Cu}^{pure} - a_{Cu}^{0} \quad (2)$$

where $a_{Cu}^{pure}$ as the lattice parameter for pure material standard, $a_{Cu}^{0}$ was the lattice parameters of Cu as a function of Nelson-Riley parameters for the respective peaks obtained from XRD patterns. The amount of Cr dissolved in Cu ($Cu_{Cr}$) was given by [11]:

$$Cu_{Cr} = \frac{\Delta a}{2.6 \times 10^{-4}} \quad (3)$$

A supersaturated solid solubility of Cr in Cu (1.96 at. %) was obtained, which was higher than the maximum solid solubility of Cr in Cu (0.77 at. %) at the eutectic temperature [12]. The decrease in $a_{Cu}^{0}$ was ascribed to that some FCC Cu atoms were replaced by BCC Cr atoms, so a substitutional solid solution was formed. Radius of Cr (1.24 Å) was smaller than that of Cu (1.28 Å) [13], therefore, the Cu lattice was contracted.

Fig. 2a illustrates the BSE images of the cross-section of the sample, and the depth of the melt layer was 290 ± 20 μm. In the substrate, dark elliptical Cr phase with average size about 90 μm is completely or incompletely surrounded by bright Cu phase, which is closely related to the complete and incomplete wetting of grain boundaries (GBs) by the melt. The incompletely wetted GBs are visible, which was also found in Zn-Al eutectic system [14]. As shown in Fig. 2b, many Cr dots dispersed in the Cu matrix, and almost all GBs are completely wetted. LSM causes intensively wetting of phase boundaries, since melting and crystallization of the surface layer were involved in the process, the wetting of GBs is apparently complete when the amount of liquid phase is high [15]. TEM bright-field (BF) image (Fig. 2c) reveals that numerous droplet-shaped Cr-rich spheres dispersed in the Cu matrix, and the average size of the spheroids was ~40 nm. The matrix ε-Cu is confirmed by indexing the corresponding selected area electron diffraction (SAED) patterns (Fig. 2d). As presented in Fig. 2e, nano-sized Cr-rich particle contain significant Cr (78.75 wt%), which is in excess of the solubility limit. The collisions between Cr-rich particles were observed, smaller Cr-rich particle (A) tended to crash into a bigger particle (B).

The formation of refined spheroidal Cr-rich particles indicates that LPS occurred in the process. CuCr30 is a pseudo alloy made of two independent phases, i.e., BCC Cr and FCC Cu with low solubility and no interphase between them. The process of melting and solidification happened at their respective melting points. At 1355 K, the Cr phase is in the solid state, the latent heat is only part of Cu. When the temperature rises to 2133 K, the Cu phase is completely fused and only the latent heat of Cr is considered. As shown in Fig. 1, clearly, the Cr phase was fully melted in the Cu matrix. The latent heat of solid-liquid phase transition at different temperatures was listed in Table 1. The cooling rate was calculated by Eq. (4) [16]:

$$\frac{dT}{dt} = -\frac{2\pi K v (T - T_0)^2}{A(q - 2r_B z_m v L)} \quad (4)$$

where K = 341 W/m·K is thermal conductivity, v = 8 m/min corresponds to the laser scanning velocity, T = 2133 K and $T_0$ = 288 K are the melting temperature and room temperature, A = 0.2 is absorptivity for the laser beam, $r_B$ = 50 μm is the beam radius, $q = \pi Q r_B^2$ is the laser power, $z_m$ = 300 μm is the thickness of the layer, and L = 1.01 × $10^9$ J/$m^3$ is the latent heat per unit volume. The calculated cooling rate for LSM sample was 5.75 × $10^6$ K/s. The high cooling rate during which could induce a dynamic undercooling (ΔT) up to 150 K, while the critical ΔT required to trigger LPS for Cu-30Cr (wt%) alloy was only 27 K [12]. Therefore, the Cu-Cr30 melt was highly undercooled.

As a result, the Cu-Cr melt is thermodynamically unstable and can enter into the liquid metastable immiscible region. The melt separates into Cu-rich ($L_1$) and Cr-rich ($L_2$) liquid. Once it starts, LPS will take place extremely fast due to high diffusivity in the liquid. $L_1$ and $L_2$ will follow their own path to finish nucleation and growth. Energy barrier to nucleation for $L_2$ was lower than that of the $L_1$ for its undercooling below the binodal line of liquidus temperature is considerably larger, so the nucleation occurred first in $L_2$. And the critical nucleation radius of Cr-rich particles is greatly reduced due to big ΔT [17]. Then $L_2$ spontaneously shrinks into numerous spherical droplets due to surface tension and solidified Cr-rich spheroids will be enveloped by the surrounding Cu melt which will solidify later.

Due to the high Q adopted in this study, fast melting concentrated near the surface, which weakened the convection of the

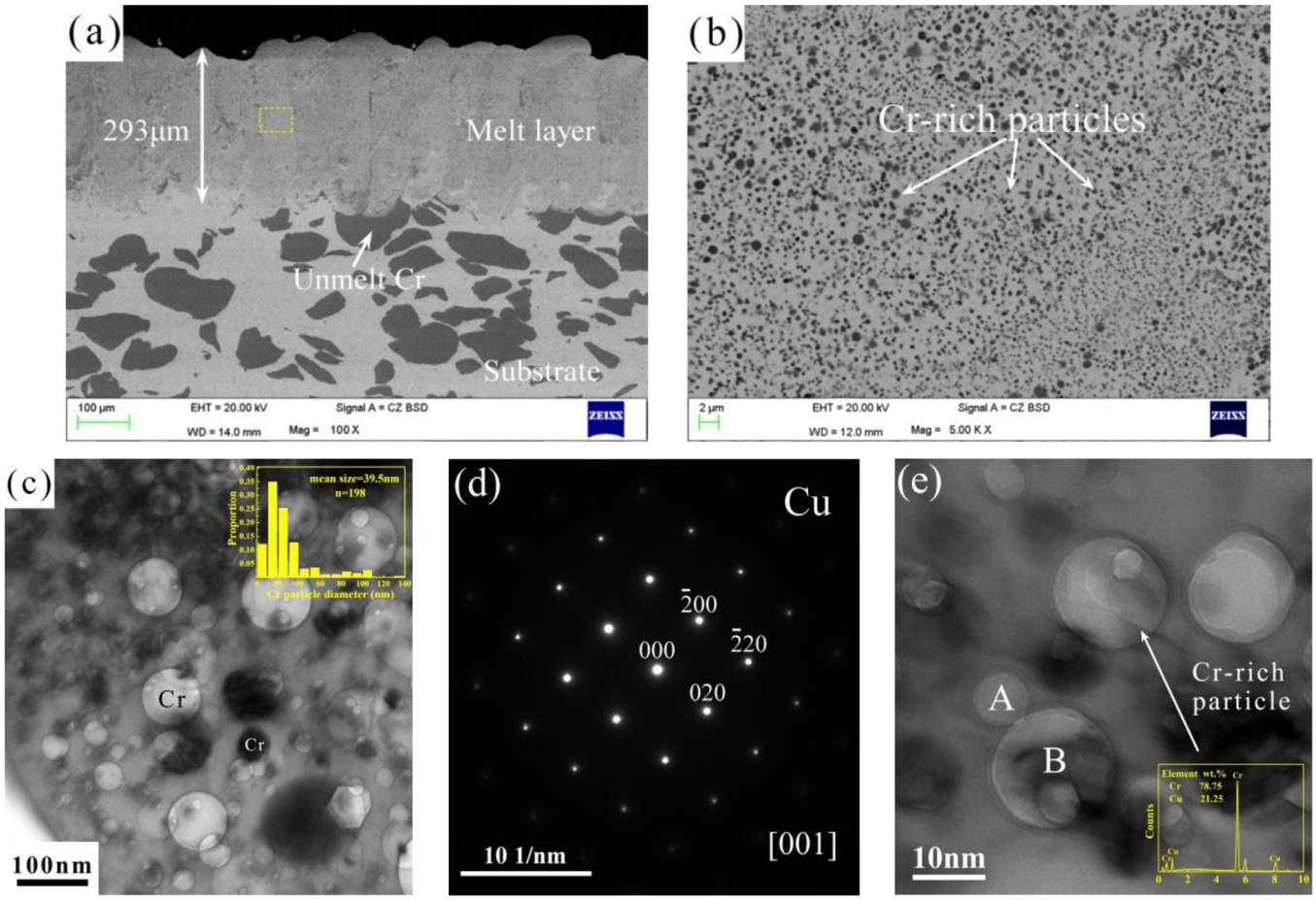


**Fig. 2.** Cross-sectional BSE image of LSM treated sample (a) the overall view, (b) magnified image of dash yellow frame in (a), (c) bright field TEM images showing Cr-rich spheroids in the layer, (d) SAED patterns in (c), (e) magnified image of Cr-rich particles. (For interpretation of the references to color in this figure legend, the reader is referred to the web version of this article.)

**Table 1**
Latent heat of Cu, Cr and Cu-30Cr alloys.

| Material | Density ($10^3$ kg/m$^3$) | Latent heat of melting/(J·kg$^{-1}$) |
|---|---|---|
| Cu | 8.9 | $2.05 \times 10^5$ |
| Cr | 7.2 | $4.02 \times 10^5$ |
| Cu-30Cr | 8.4 | 1356 K: $0.7 \times 2.05 \times 10^5$<br>2133 K: $0.3 \times 4.02 \times 10^5$ |

melt pool. And the effect of Marangoni motion and Stokes were feeble when the diameter of Cr-rich particles were <1μm (Fig. 2b and c). The random migration of nano-scaled Cr-rich particles is mainly dominated by Brownian motion [18]. Nano Cr-rich particles are constantly impacted by Cu atoms and other Cr-rich nanoparticles when they suspended in the melt. These collisions change the directions and velocities of the Cr-rich particles. However, the liquid miscibility gap is very narrow for Cu-Cr30 (wt%), and the cooling rate is so high that there existing little time for the melt to pass through the gap. Therefore, the collisions between Cr-rich particles were insufficient, so nano-scaled Cr-rich particles solidified in the Cu matrix without continuous grain growth.

## 4. Conclusions

Stable and reliable large area surface nanocrystallization of Cu-Cr30 (wt%) was achieved by a continuous laser beam with high power density ($1.08 \times 10^7$ W/cm$^2$). The microstructure was characterized by nano-sized Cr-rich spheroids (~40 nm) dispersed in the Cu-rich matrix. Due to fast heating and rapid cooling ($5.75 \times 10^6$ K/s) in the process, insufficient LPS shortened the moving time for Cr-rich spheroids. Meanwhile, the movements of Cr-rich particles were dominated by Brownian motion which weakened the enrichment effect. Therefore, the sizes of Cr-rich spheroids were maintained at nano scale.

## Acknowledgement

This work was supported by the instrument developing project of the Chinese Academy of Sciences (No. yz201636) and the plan of Beijing Municipal Commission of Science and Technology (Z181100003818015).

## References

[1] S. Bahla, S. Suwasa, T. Ungàrb, K. Chatterjee, Acta. Mater. 122 (2017) 138–151.
[2] J.K. Han, X. Li, R. Dippenaar, K.D. Liss, M. Kawasaki, Mat. Sci. Eng. A. 714 (2018) 84–92.
[3] I. Yamada, N. Toyoda, Surf. Coat. Technol. 201 (2007) 8579–8587.
[4] S. Lou, Y. Li, L. Zhou, X. Nie, G. He, Y. Li, W. He, Mater. Design. 104 (2016) 320–326.
[5] J. Liu, S. Suslov, Z.C. Ren, Y.L. Dong, C. Ye, Int. J. Mach. Tool. Manu. 136 (2019) 19–33.
[6] C.Y. Cui, J.D. Hu, Y.H. Liu, K. Gao, Z.X. Guo, Appl. Surf. Sci. 254 (2008) 6779–6782.
[7] Md.S. Ahsan, F. Ahmed, Y.G. Kim, M.S. Lee, M.B.G. Jun, Appl. Surf. Sci. 257 (2011) 7771–7777.
[8] X.G. Cui, C.Y. Cui, X.N. Cheng, X.J. Xu, J.Z. Lu, J.D. Hu, Y.M. Wang, Mat. Sci. Eng. A. 527 (2010) 7400–7406.

[9] J. Mazumder, Opt. Eng. 30 (1991) 1208–1219.
[10] C. Suryanarayana, Prog. Mater. Sci. 46 (2001) 1–184.
[11] M.J. Tenwick, H.A. Davies, Mater. Sci. Eng. A. 98 (1988) 543–546.
[12] K.T. Jacob, S. Priya, Y.A. Waseda, Z. Metallkd, Z. Metallkd. 91 (2000) 594–600.
[13] T.P. Harzer, S. Djaziri, R. Raghavan, G. Dehm, Acta. Mater. 83 (2015) 318–332.
[14] B.B. Straumal, A.S. Gornakova, O.A. Kogtenkova, et al., Phys. Rev. B 78 (2008) 054202.
[15] A.B. Straumal, B.S. Bokstein, A.L. Petelin, B.B. Straumal, et al., J. Mater. Sci. 47 (2012) 8336–8343.
[16] J. Zhang, X. Cui, Y. Yang, Y. Wang, Metall. Mater. Trans. A. 44 (2013) 5544–5548.
[17] S. Curiotto, N.H. Pryds, E. Johnson, L. Battezzati, Mater. Sci. Eng. A. 449–451 (2007) 644–648.
[18] N. Liu, F. Liu, W. Yang, Z. Chen, G.C. Yang, J. Alloy. Compd. 551 (2013) 323–326.